Materials Science and Engineering Faculty
Research & Creative Works

Materials Science and Engineering

05 Apr 2018

Efficiency of Solid Inclusion Removal from the Steel Melt by Ceramic Foam Filter: Design and Experimental Validation

Soumava Chakraborty

Ronald J. O'Malley
Missouri University of Science and Technology, omalleyr@mst.edu

Laura Bartlett
Missouri University of Science and Technology, lnmkvf@mst.edu

Mingzhi Xu

Recommended Citation

Efficiency of Solid Inclusion Removal from the Steel Melt by Ceramic Foam Filter: Design and Experimental Validation

Soumava Chakraborty, Ronald J. O'Malley, Laura Bartlett, Mingzhi Xu

Peaslee Steel Manufacturing Research Center, Department of Materials Science & Engineering

Missouri University of Science and Technology, Rolla, MO, USA-65409

ABSTRACT

An investigation was performed to measure the efficiency of solid alumina inclusion removal by filtration during casting. A mold design was developed using modeling software to produce two castings that fill simultaneously, one with a filter and the other without a filter. The design avoided vortex formation and thus air entrainment, which helped to avoid reoxidation inside the mold cavity. Samples from these castings were analyzed utilizing an SEM/EDS system with automated feature analysis (AFA) to measure the efficiency of inclusion removal using a 20 ppi zirconia foam filter. This study also documents the occurrence of inclusion flotation and agglomeration in the ladle which, in turn, affects the removal efficiency of these inclusions by filtration in the mold.

Keywords: steel, non-metallic inclusions, ceramic filter, mathematical modeling

INTRODUCTION

Non-metallic inclusions in steel can reduce mechanical properties, produce surface defects, affect machinability and increase scrap rate[1]. In foundry steelmaking, ceramic filters have been used to remove these inclusions for years. Several studies show that ceramic filters can effectively remove inclusions[2-4] from the steel melt. The melt flow rate inside the mold cavity influences the inclusion removal by filtration. Higher flow rates[4] or melt velocities[5] through the filter lowers the inclusion removal efficiency (η), which can be defined as:

$$\eta = \frac{C_i - C_o}{C_i} \qquad \textbf{\textit{Eqn. 1}}$$

where, C_i and C_o are the inclusion concentration in the steel melt at the inlet and at the outlet respectively. Filter geometry also plays an important role on inclusion removal. An increase in filter thickness[6] or aspect ratio[7] increases the inclusion removal efficiency due to an increased residence time in the filter. A direct comparison of filtered and unfiltered castings from the same heat having same inclusion content has not been studied extensively. The objective of the current study is to evaluate the effectiveness of solid alumina inclusions filtration from steel by comparing castings produced with and without a filter from the same heat. The study by Raiber et al.[4] has indicated that foam filters have a higher filtration efficiency compared to multi-hole filters and loop filters. Consequently, foam filters were selected for this study.

MATHEMATICAL MODELING AND DESIGNING

A mathematical model was developed using computational fluid dynamics (CFD) simulations of fluid flow and heat transfer during mold fill for a 316 stainless steel using MAGMA 5.3. The casting and rigging design is shown in Figure 1. Two modified Y-block castings are shown in vertically parted no-bake molds in Figure 1: one filtered (by a FOSECO STELEX ZR 10 ppi filter: 10 cm X 10 cm X 2.5 cm) and another unfiltered.

In a previous study, Raiber et al.[4] showed that multi-hole filters and loop filters can remove large alumina inclusions from steel, but that ceramic foam filters remove these inclusion particles more effectively than multi-hole filters or loop filters. They reported a maximum inclusion removal efficiency of 95% for a 25 ppi foam filter in their experiments.

In the present CFD model, it has been found that a 25 ppi foam filter creates excessive resistance to liquid metal flow during mold fill and creates a risk of freezing during filling. For this reason, a 10 ppi foam filter was used to avoid excessive filling resistance and allow simultaneous filling of both the filtered and unfiltered castings. The size of the filter was selected to maximize the residence time in the filter, which increases the filtration efficiency.

MgO stabilized zirconia foam filters were employed in our experiments, Figure 2, because they are chemically inert to molten steel.
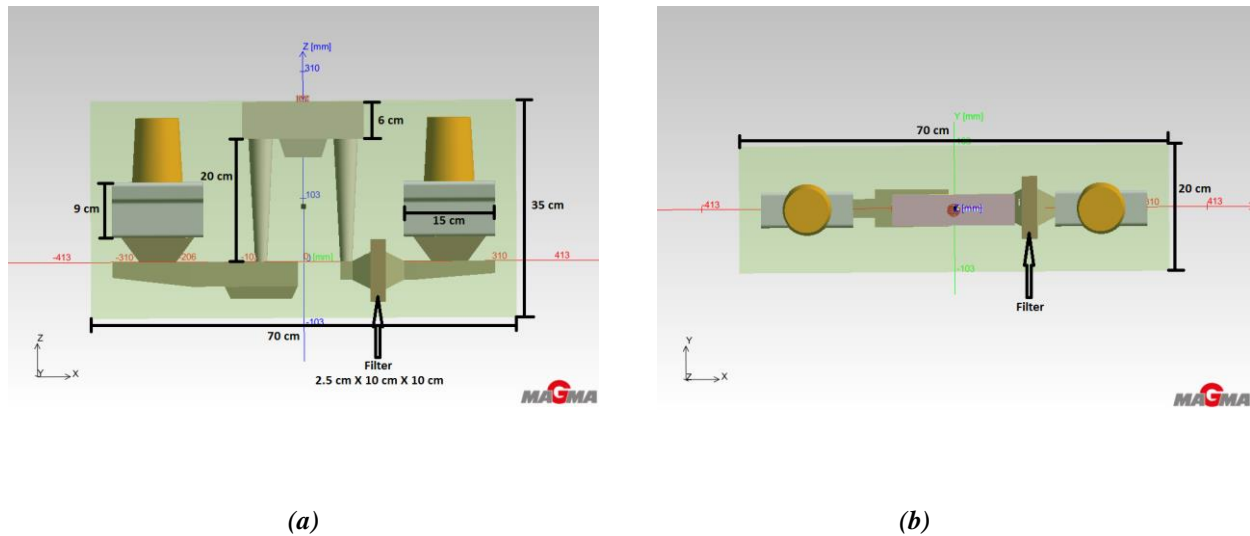

(a)   *(b)*

Figure 1. MAGMA 5.3 drawing of mold and rigging system: (a) front view and (b) top view

Both sides of the castings were designed to be filled by a common pouring cup so that the physical properties and composition of liquid steel remain same for both the sides. By characterizing the samples from both these sides, a direct comparison can be made between the filtered and non-filtered castings and the effectiveness of the zirconia filter on inclusion removal can be determined. A dam is attached under the pouring cup to reduce the melt velocity and air entrapment. Bottom filling has been adopted to minimize the reoxidation of the melt.

The dimension of the mold is 70 cm x 20 cm x 35 cm. To minimize the back pressure during pouring two separate sprues are fed from a single pouring cup to fill the two castings simultaneously. Sprue diameters were also optimized to minimize air entrapment during mold filling. The dimensions of the sprues, gates, castings and risers from both sides are same, although the runners are different to adjust the liquid metal flow rate and ensure a simultaneous filling in the mold cavities for both sides. Hence, the gating ratios are different for both sides: 1:2:3.8 (with filter) and 1:2.6:3.8 (without filter).This design also minimizes vortex formation inside the mold.

Filling velocity, time and temperature were predicted for this design using the mold filling and solidification software as shown in Figure 3. Solidification parameters were also evaluated by the software to ensure that the castings were sound. The castings were predicted to be free of porosity.

Figure 2. Zirconia foam filter: 10 ppi (10 cm X 10 cm X 2.5 cm).

Decreasing the velocity inside the mold cavity decreases the turbulence created by the liquid metal during filling which in turn decreases reoxidation of the melt. For steel, the recommended maximum velocity to minimize surface turbulence is less than 0.45 m/s[8].

For this mold design, the minimum filling time was found to be 9 s. Below this, a separation of metal stream was observed at the entrance of the castings. This type of discontinuity in the liquid can entrain air and create reoxidation inclusions. With this minimum pouring time, a moderate pouring rate of 2.9 kg/s was targeted for the mold.

The metal flow patterns during filling are different for the two different gating systems (with and without filter). The side without the filter initially showed a higher velocity as no filter was present to restrict the flow of the melt. To compensate for this, a sprue well was added to the side without the filter as shown in Figure 1. The metal entering the runner has a lower velocity than in the sprue. For most of the pouring time, the velocity in the runner is less than 0.4 m/s. At the gate, the liquid metal changes its direction and due to a sudden release in pressure, the velocity increases.

which is higher than the liquidus temperature of 316 stainless, 1371-1399°C, depending on the specific composition of the steel.

Lowering the pouring rate or increasing the pouring time to greater than 9 s gives lower velocities inside the mold cavity. However, longer filling time can also cause air entrainment into the liquid metal stream during pouring, which would interfere with the experimental objectives. Slow filling can also create a temperature drop and premature
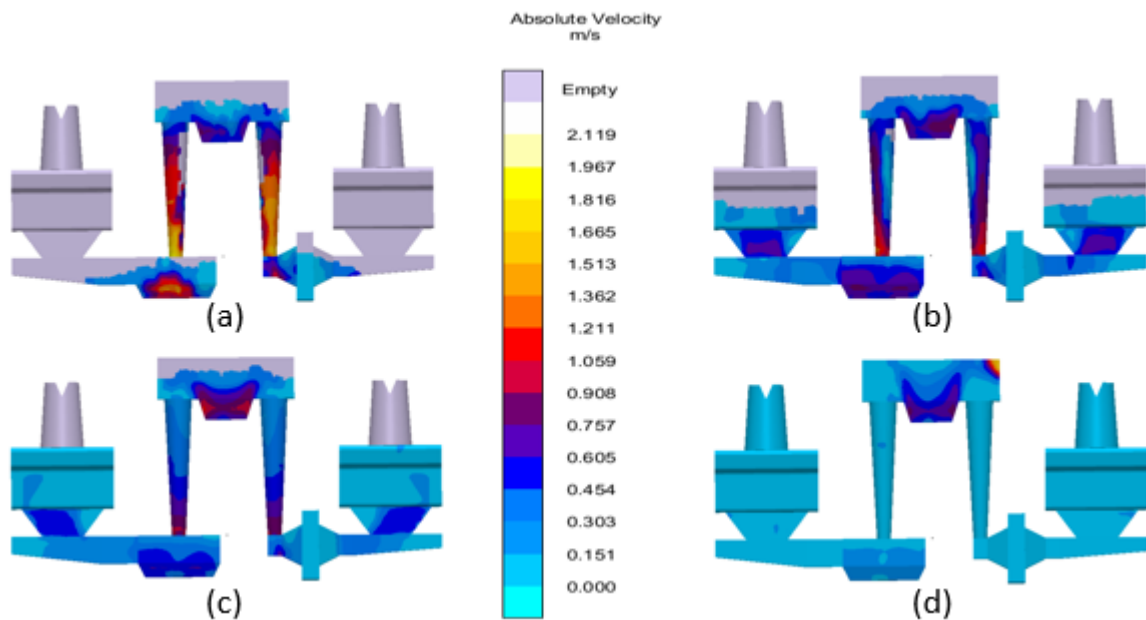

Figure 3. Absolute velocity of the steel melt at: (a) 25% (b) 50% (c) 75% and (d) 100% filling of mold.

The volume of the gate is small compared to the overall volume of the mold cavity. Therefore, the risk of air entrainment in gates is minimal. In the casting, the absolute velocity decreases and is less than 0.45 m/s at all times during the fill as shown in Figure 3. Tracer particle tracking in the filling and solidification software also demonstrates that minimal vortexing is generated in the mold during the filling.

The filling time for these two sides are designed to be the same to avoid any back pressure generation at one side of the mold during the filling and to ensure that steel from the ladle reaches both molds simultaneously. To match the filling times, the gating ratio on the side without the filter was adjusted to balance the fill times. As shown in Figure 4.(a), both the sides are filled at the same time. The pouring temperature was set to 1550°C and the temperature during filling has also been modeled as shown in Figure 4.(b). The minimum steel temperature predicted during filling is 1502°C

solidification inside the mold cavity before completion of filling. This may result cold shuts or misruns. Therefore, for experimental studies these two opposing factors were always considered and in the current study the pouring time was maintained below 15 s, which shows a slower filling (than that of minimum pouring time) with lower filling velocities below the critical value of 0.45 m/s to avoid any premature solidification.

EXPERIMENTAL PROCEDURE

Three molds were prepared from a 3D-printed pattern as shown in Figure 5.(a). The patterns for the design were 3D-printed with acrylonitrile butadiene styrene ($(C_8H_8 \cdot C_4H_6 \cdot C_3H_3N)_n$) polymer. All the parts were finish sanded with emery paper and glued into the mold box (Figure 5.(a)). Before molding, the mold box along with the 3D-printed parts are coated with a release agent, ZIP-SLIP® LP 78 and then allowed to dry for 24 hours.

To fit the risers into the mold cavity, cylindrical cores were added. Using these patterns, no-bake sand molds were constructed to carry out the experiments as shown in Figure 5.(b).

bottom of the teapot ladle filled up the first mold, melt from the middle filled up the second mold, and melt from the top part of the ladle filled up the third mold (Figure 6.(b) and (c)). Hence, by determining the size and distribution of the
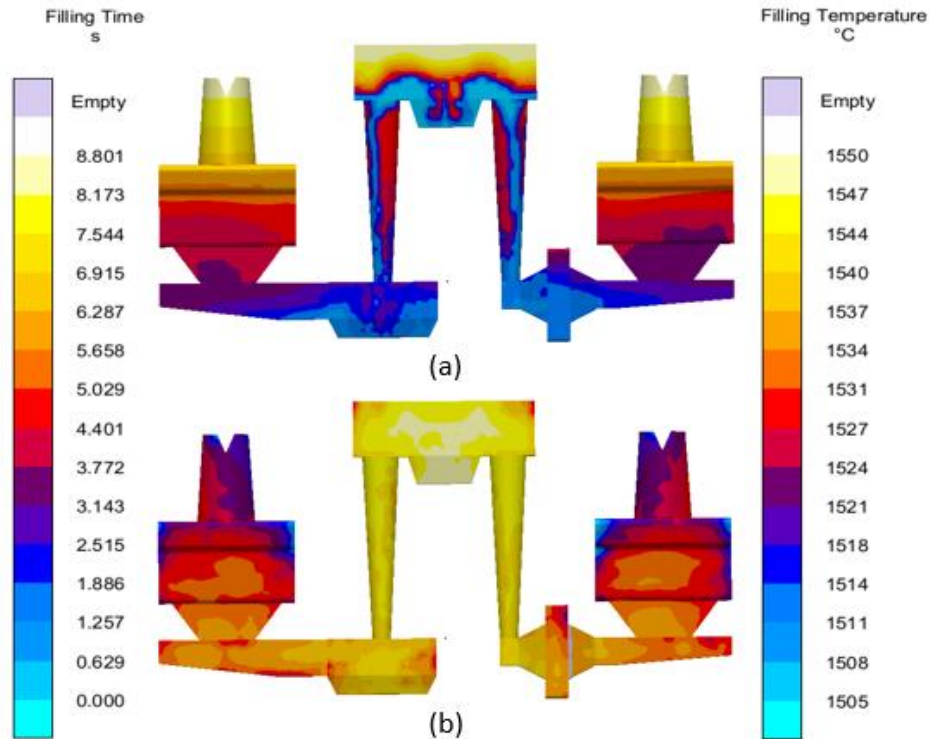

Figure 4. (a) Filling time and (b) filling temperature at the end of filling of the steel melt at different positions.

Steel heats were prepared in a 200 lbs coreless induction furnace under argon cover. Figure 6.(a) shows a photograph of the induction furnace and three vertically parted molds prior to casting. 176 lbs (80 kgs) of 316 stainless steel charge stock was induction melted under a continuous argon gas flow (15 SCFH). At 1548°C, a chemistry sample was taken. At 1644°C the steel melt was tapped into a preheated teapot-style ladle as shown in Figure 6.(b and c).

Because the objective of this study was to understand the efficiency of filtration of solid inclusions, aluminum was used as the deoxidizer (0.1wt% of the melt). The deoxidizer was submerged into the ladle with a steel rod and then vigorously stirred. After the addition of deoxidizer, another chemistry sample was taken from ladle before pouring. Finally, the molten metal was poured into three molds at 1554°C.

Inclusion floatation in the ladle during teeming was studied using three molds (Figure 6.(a)) that were filled from a single ladle. The metal from the

inclusions in the resulting castings and gating systems, the extent of inclusion flotation and agglomeration in the ladle could be determined.

RESULTS

Castings from the three different mold sets were examined thoroughly and no blow-holes, pin-holes, surface cracks, misruns or cold shuts were found. Chemical analysis of the samples taken during experiments was carried out using optical emission arc spectroscopy and LECO combustion method (CS 600 and TC 500). The chemistries of the melt before and after deoxidation are shown in Tables 1 and 2, respectively. It can be the observed that aluminum content in the ladle is increased by 0.1% due to the addition of deoxidizer in the melt. To characterize the inclusion population of the castings, samples were taken from different position of the castings as shown in Figure 7. A scanning electron microscope, SEM, (ASPEX PICA 1020) with energy dispersive X-Ray spectroscopy, EDS, and automated feature analysis

(a)   *(b)*

Figure 5. (a) 3D-printed patterns in a wooden flask and (b) corresponding half of a vertically parted no-bake sand mold.

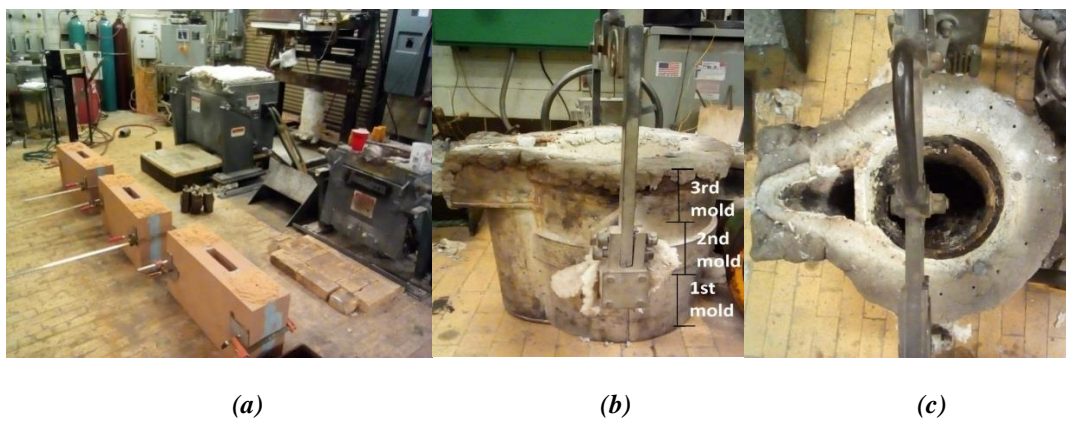*(a)*   *(b)*   *(c)*

Figure 6. (a) Three mold sets, (b) 200 lbs teapot ladle (side view) and (c) 200 lbs teapot ladle (top view).

Table 1. Melt composition before 0.1 wt% Al addition (sample taken from furnace).

C	Si	Mn	Al	Cr	Ni	Mo	Cu	Ti	N	P	S	O
0.063	1.37	0.51	0.013	18.57	9.03	2.47	0.24	0.012	0.063	<0.0016	0.0039	0.0354

Table 2. Melt composition after 0.1 wt% Al addition (sample taken from ladle during pouring).

C	Si	Mn	Al	Cr	Ni	Mo	Cu	Ti	N	P	S	O
0.084	1.40	0.52	0.12	18.67	9.00	2.47	0.23	0.014	0.085	<0.0016	0.0044	0.0188

(AFA) was utilized to characterize the composition, size, and distribution of inclusions.

Samples 1 and 2 were collected from the upper part of castings, samples 3 and 4 were collected from the two runners and samples 5 and 6 were collected before and after the filter as shown in Figure 7.

The effect of the filter can directly be compared from samples 5 and 6. Sample 5 corresponds to the inclusion population of incoming liquid stream,
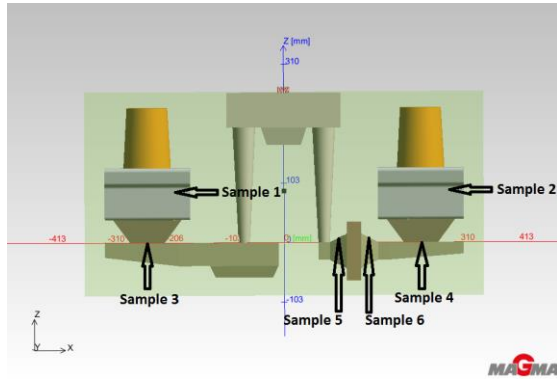

Figure 7. Sampling positions for metallography and inclusion analysis.

whereas sample 6 is from the outgoing liquid stream after the filtration. From the other samples, the effect of runner design (comparing sample 6 to 4) and floatation (comparing sample 4 to 2) can be determined. Metallographic specimens were prepared by sectioning and polishing utilizing standard metallographic techniques. Samples from positions 1-6 were prepared for metallography and inclusion analysis.

The SEM/EDS AFA study also showed that the inclusions in the sample were uniformly distributed. A representative figure is shown here for sample 3 from the third mold set (Figure 8).

Total oxygen content of samples 5 and 6 from molds 1 and 3 was calculated from the total amount of oxide inclusions as determined by inclusion analysis. These values were then compared with total oxygen contents determined by combustion method (Figure 9). In both of these analyses the total oxygen content was decreased from sample 5 to sample 6 and this was expected as alumina inclusions were removed by the filter. As for both the techniques, the trends are similar and analysis of inclusions by the SEM/EDS AFA technique can be considered reliable.

The inclusion populations were measured for all the samples along with their chemistry, position, and size. For all the samples, alumina, manganese sulfide (MnS) and some complex inclusions (mainly MnS that heterogeneously precipitated on preexisting alumina) have been observed as shown in Figure 10.

A joint ternary diagram is presented in Figure 11 and shows the nominal chemistry and size distributions of the different types of inclusions.
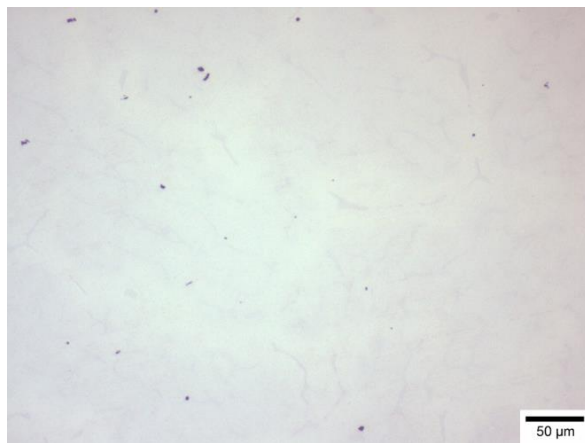
(a)
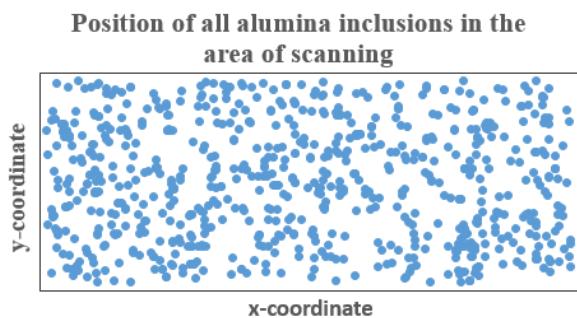
(b)

Figure 8. (a) Inclusions found by optical microscopy (Sample 3, third mold) and (b) cluster analysis using SEM/EDS data (Sample 3, third mold).

Before performing the inclusion analysis, the samples were examined under an optical microscope. From this study, it was observed that the inclusions were randomly distributed.

Manganese sulfide inclusions were mainly observed near the grain boundaries of the castings and these were formed during and after solidification. The size of this type of inclusion formation strongly depends on the solidification
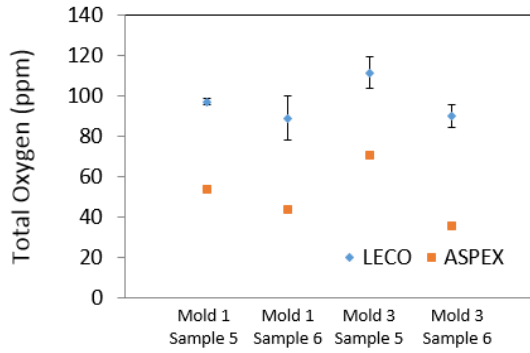
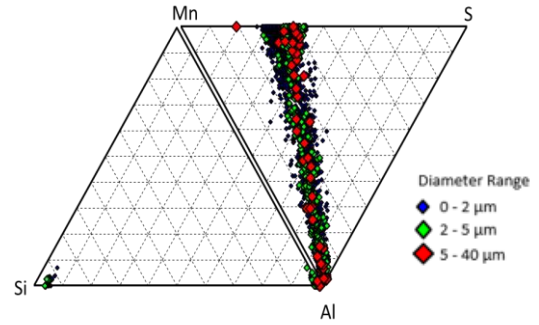*Figure 9. Total oxygen measured at different sampling positions with LECO and ASPEX.*

Figure 11. Joint ternary diagram of the inclusions observed for Mold 1, Sample 1.
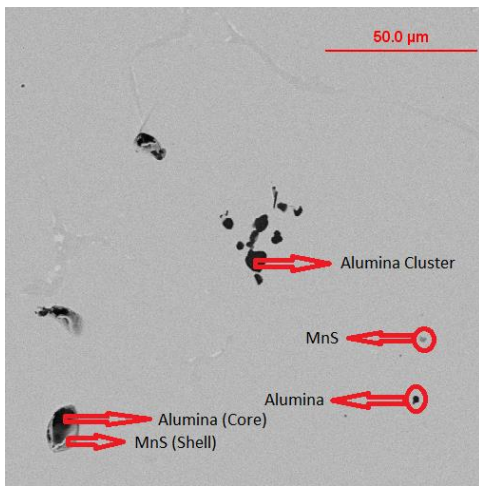

Figure 10. Backscattered electron image of different inclusions observedin this analysis.

rate of the castings, which is a variable parameter at different positions. MnS inclusions were also associated with alumina inclusions, sometimes forming complex inclusions which can interfere with the statistical analysis of the oxide inclusions of interest that were present in the melt. To solve this problem, a threshold filter was applied to only consider the inclusions with high Al content. For aluminum content $\geq$ 90%, all the inclusions were considered as pure alumina. Considering this assumption, area fraction of the alumina inclusions (in ppm) was calculated (Figure 12).
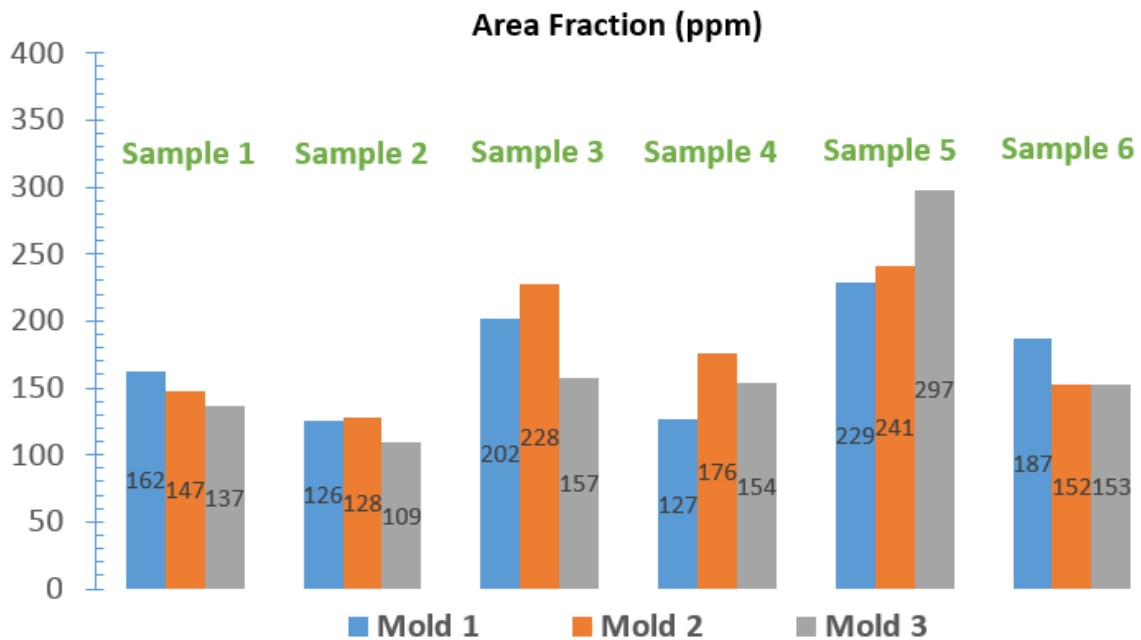

Figure 12. Area fraction of the alumina inclusions for Samples 1-6 for all three molds.
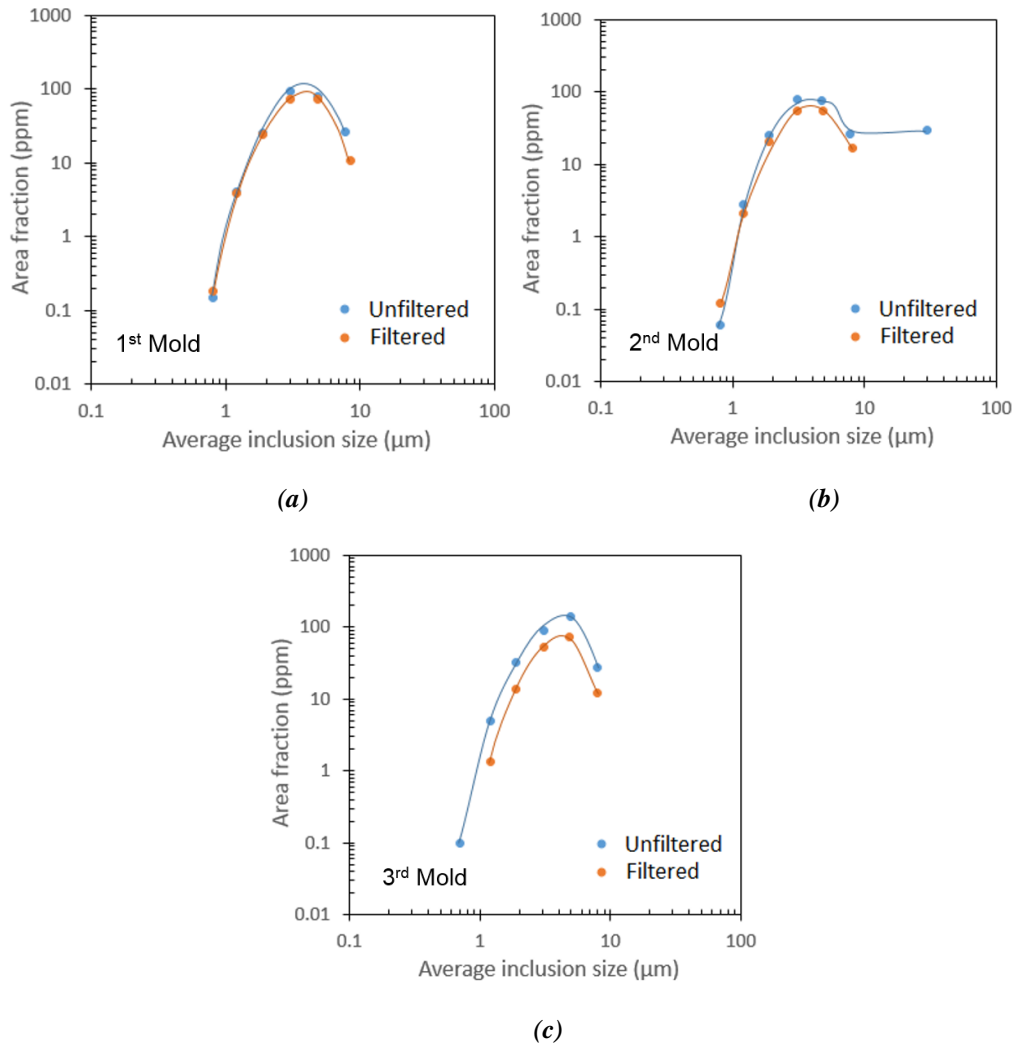
(a)

(b)

(c)

Figure 13: Size distributions of alumina inclusions before and after filtration. Samples 5 & 6 indicate removal of inclusions from the: (a) first mold, (b) second mold and (c) third mold.

DISCUSSION

Comparing unfiltered and filtered samples 1 & 2, 3 & 4 and 5 & 6 for all the mold sets, it can be observed that solid alumina inclusions can effectively be removed after filtration as shown in Figure 12. It can also be observed that the incoming steel before filtration (Sample 5) contained a greater number of alumina inclusions when compared to the other samples collected. For all the three molds, the area fraction (in ppm) for Sample 5 of third mold shows the highest value (297 ppm) followed by second mold (241 ppm) and third mold (229 ppm). This is to be expected as alumina inclusions are lighter than the steel melt and have a tendency to float towards the top of the teapot style ladle. Size distribution of alumina inclusions from just before the filter (sample 5) and just after the filter (sample 6) are shown in Figure 13 for the different molds that were poured. From the size distribution analysis of these inclusions, it

can be determined that mold 3 shows the maximum number of larger inclusions (5-10 µm), followed by mold 2 and mold 1. This is anticipated, as alumina inclusions tend to agglomerate and float to the top of the ladle. Therefore, the last metal poured should contain the steel with the highest oxide content.
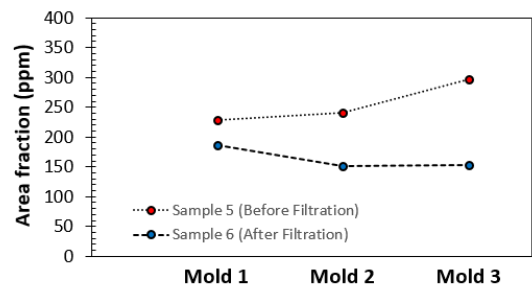

Figure 14. Area fractions of the alumina inclusions for Samples 5 (before filtration) and 6 (after filtration) for all three molds.

Comparing the area fractions of Sample 5 and 6 for all three molds (Figure 14), it can be seen that for mold 3, the inclusion removal is a maximum of 48% followed by mold 2 at 37% and mold 1 at 18%. The increase in incoming inclusion content with time is a direct result of the floatation and agglomeration of alumina inclusions in the ladle with time. In addition, the filtration efficiency (Figure 14) improves with ladle hold time and increasing incoming inclusion content. Also, it appears that the top of the ladle contains a higher concentration of slightly larger alumina inclusions, which have a better chance of being captured by the filter and removed.

The filtration efficiency numbers reported in this study are somewhat lower than the 68% efficiency reported in a previous study by Raiber et. al.[4]. However Raiber's experiment employed a finer 25 ppi foam filter and calculated the efficiency using measurements of total oxygen content. Differences in mold setup, orientation of the filter, composition of the filter, alloy composition and the initial inclusion concentration may also explain the differences in observed filtration efficiency.

Considering sample 6 (just after the filter), mold 1 has the highest inclusion content, 187 ppm, compared with mold 2 at 152 ppm, and mold 3 at 153 ppm. This is because the alumina inclusions entering the filter are slightly smaller and at a lower incoming inclusion concentration.
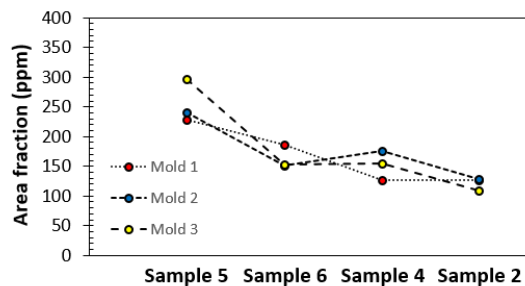

Figure 15. Area fractions of the alumina inclusions for Samples 5, 6, 4 and 2 for all three molds.

From Sample 4 to Sample 2, a drop can be seen in the area fraction of the inclusions for mold 2 (27%) and mold 3 (29%). This is due to the floatation of the inclusions towards the risers during filling (Figure 15). For mold 1, the inclusions are slightly smaller and they are not as likely to float.

It can also be observed from Sample 5 and Sample 2 that the area fraction of the inclusions decreased by 45%, 47% and 63%, respectively for mold 1, mold 2 and mold 3 (Figure 15). This decrease

indicates that the overall decrease in inclusion content is the result of a combination of filtration and floatation of the inclusions inside the mold cavity. It also suggests that the larger inclusions are more likely to be removed by the combination of filtration and floatation.

CONCLUSIONS

A mold design and an appropriate rigging system has been designed using mold filling and solidification software to study the filtration efficiency of solid alumina inclusions removal by a ceramic foam filter. This design employs two Y-block castings in the same mold, one with and other one without a filter in the runners. In this current design, liquid steel fills the mold cavity from the bottom with minimum vortex formation and turbulence, which reduces air entrainment. CFD modeling of the test configuration shows that for both of the castings, filling time is matched for both sides. Misruns and cold shuts were avoided. An experiment with three different mold sets has been carried out using three molds that were filled from a single heat to observe the effects of inclusion stratification in the ladle at the same time that the filtration efficiency is evaluated. From this experiment, the following conclusions can be made:

1. Stratification of solid alumina inclusions was observed in the ladle due to floatation of inclusions towards the top of the ladle after aluminum killing. Using a bottom pour 'teapot' ladle, successively teemed molds were observed to have increasing incoming inclusion concentrations.
2. Zirconia (10 ppi) foam filters effectively remove the alumina inclusions from steel melt. In this experiment, mold 3 had the highest incoming concentration of inclusions and also the highest overall inclusion removal efficiency (48%) by filtration.
3. Floatation of inclusions (5-10 µm) inside the mold cavity also contributed to inclusion removal. Molds 2 and 3 showed the removal of inclusions due to floatation in the mold cavity, whereas mold 1 did not.
4. Both filtration and floatation mechanisms appear to play an important role for inclusion removal. The combined effect is larger than filtration alone. In this study, the highest combined inclusion removal efficiency observed in mold 3 was 63%, with filtration accounting for 48% of the removal efficiency.

FUTURE WORK

Filtration of solid alumina inclusions was considered in this study. Future experiments utilizing the same mold and casting design will be conducted to study the removal efficiencies of liquid manganese-silicate inclusions and liquid calcium-modified alumina inclusions.

Examination of the filter media by metallographic methods is planned to observe the inclusion attachment mechanisms and the distribution of the inclusions through the body of the filter for both liquid and solid inclusions.

Notch toughness of filtered and unfiltered castings will be evaluated in these and future trials using Charpy V-notch testing.

The effects of different filter orientations and filter types on inclusion removal efficiency will also be investigated.

ACKNOWLEDGMENTS

REFERENCES

1. Simmons, W., Broome, A.J., "Influence of Metal Filtration on the Production of High Integrity Cast Products," SEAISI Thailand Conference, Bangkok, pp. 47 (May 1987).
2. Apelian, D., Mutharasan, R., Ali, S., "Removal of Inclusions from Steel Melts by Filtration," *Journal of Materials Science*, 20, pp. 3501 (1985).
3. Janiszewski, K., Kudlinski, Z., "The Influence of Non-Metallic Inclusions Physical State on Effectiveness of the Steel Filtration Process," *Steel Research International*, 77(3), pp. 169 (2006).
4. Raiber K., Hammerschmid, P., Janke, D., "Experimental Studies on Al_2O_3 Inclusions Removal from Steel Melts Using Ceramic Filters," *ISIJ International*, 35(4), pp. 380 (1995).
5. Ali, S., Mutharasan, R., Apelian, D., "Physical Refining of Steel Melts by Filtration" *Metallurgical Transaction B*, 16B, pp. 725 (1985).
6. Tian C., "On the Removal of Non-Metallic Inclusions from Molten Steel through Filtration," PhD Thesis, McGill University (1990).
7. Janiszewski K., "Influence of Slenderness Ratios of a Multi-Hole Ceramic Filters at the Effectiveness of Process of Filtration of Non-Metallic Inclusions from Liquid Steel," *Archives of Metallurgy and Materials*, 57(1), pp. 135 (2012).
8. Campbell J., "Complete Casting Handbook", *Elsevier Ltd.*, Oxford, UK (2011).